Environ Res Tec, Vol. 9, Issue 3, pp. 520-534, June 2026

Environmental Research & Technology
https://ertjournal.org/index.php
DOI: https://doi.org/10.35208/ert.1647233

RESEARCH ARTICLE

Valorisation of biochar from poultry litter power plant to activated carbon: Production, characterisation, and application

Gamze DOĞDU YÜCETÜRK [1], Turgay PEKDEMİR [2,3,*], Elif ÇELİK [4], Murat DOĞRU [4]

[1] *Bolu Abant Izzet Baysal University, Faculty of Engineering, Department of Environmental Engineering, Bolu, Türkiye*
[2] *Bolu Abant Izzet Baysal University, Faculty of Engineering, Department of Chemical Engineering, Bolu, Türkiye*
[3] *Bolu Aban Izzet Baysal University, Innovative Food Technologies Development Application and Research Centre (YENIGIDAM), Bolu, Türkiye*
[4] *Gebze Technical University, Department of Environmental Engineering, Gebze, Türkiye*

ARTICLE INFO

Article history
Received: 27 February 2025
Revised: 30 May 2025
Accepted: 19 July 2025

Key words:
Poultry litter valorisation, biochar, activated carbon, water treatment, gasification

ABSTRACT

In support of zero-waste and circular economy principles, this study aims to develop a sustainable and value-added solution for poultry litter (PL) waste by converting it into activated carbon (AC) for environmental applications. One promising valorisation route is using biochar derived from PL to produce AC, a material with wide application and market demand. This study produced, characterised, and investigated the application of ACs from the biochar of an industrial-scale thermal gasification plant using PL as fuel. We tested some selected ACs to remove methylene blue (MB) dye from simulated wastewater. We employed physical and chemical activation with CO_2 and various ratios of H_3PO_4 and $ZnCl_2$ to produce ACs at 550 °C, 700 °C, and 800 °C. We characterised ACs by XRD, EDX, FTIR, and BET-based techniques. ACs from H_3PO_4, $ZnCl_2$, and CO_2 activation exhibited a specific surface area of 279.6, 219, and 180.6 m^2/g, respectively. MB adsorption followed a pseudo-second-order model, with a capacity of 48.6, 75.5, 119.3, and 62.2 mg/g for ACs from H_3PO_4, $ZnCl_2$, CO_2 activation, and biochar, respectively, according to the Langmuir model. Our findings emphasize the feasible production of ACs from poultry waste and their efficacy for plausible sustainable application as adsorbents, for example, in water treatment to remove dyes.

Cite this article as: Doğdu Yücetürk G, Pekdemir T, Çelik E, Doğru M. Valorisation of biochar from poultry litter power plant to activated carbon: Production, characterisation, and application. Environmental Research and Technology, 2026, 9 (3), 520-534.

INTRODUCTION

Poultry meat industry has been rapidly growing [1, 2] with the global production as 136 million tonnes in 2020 and lately accounting about 40% of the global meat production [3] which generates substantial mass of poultry litter (PL) comprising a blend of bedding material, manure, waste feed, deceased birds, damaged eggs, and chicken feathers [4]. The yearly production of PL ranges from 1.5 to 5.7 kg per bird [5], yielding about 14 million tonnes in the US and 2 billion tonnes in Europe [6]. Considering global environmental and health concerns associated with PL, such as strict EU regulations [7], finding viable and sustainable solutions is imperative.

Application of PL for soil improvement is a practical method for recycling essential plant nutrients like nitrogen (N), phosphorus (P), and potassium (K) [8]. However, the excessive use or direct discharge of PL without adequate treatment on land causes large-scale accumulation of PL with detrimental environmental and health problem consequences [9, 10]. Therefore, it is vital to address the issue of PL waste, with suitable environmental technologies which do not only not pollute the soil and ground and surface water sources but also not pose a risk to human health by degrading air quality, facilitating the spread of viral and bacterial diseases among chickens, and emitting unpleasant odours in open areas [11, 12].

Alternative to the dominant direct land application, utilization of PL for composting, incineration, pyrolysis, gasification, anaerobic digestion, and even as catalyst in wastewater treatment can offer advantages [2, 13-15]. Biochar, a lightweight porous carbonaceous residue material with a carbon content of 20% - 40%, is generated through gasification/pyrolysis processes [11, 16-18]. Biochar possesses microporous structure with vast specific surface area, numerous surface oxygen functional groups, and high cation exchange capacity (CEC) [19]. Biochar may, however, have approximately 20% ash by dry weight [20]. These inherent qualities characterize Biochar's capacity to function as an adsorbent for the remediation of gases, soils, and wastewater [21, 22]. Biochar, regardless of its origin, also has

* Corresponding Author: turgay.pekdemir@ibu.edu.tr (Turgay Pekdemir)

the potential to be converted into high-value-added products, such as activated carbon (AC) and soil conditioner [23-26].

AC typically has a high specific surface area (3000 m^2/g), surface reactivity, and porosity with no discernible taste or odour [27, 28]. These characteristics render AC a promising adsorbent in various fields such as wastewater treatment, removal of toxic and global warming contributing gases from the environment, a catalyst, and a catalyst carrier [27, 29, 30]. In March 2023, the price of AC was $6,40/ton with a monthly growth rate of +2.1% from the previous year [31]. The global market for AC in 2024 has been estimated to be $7.21 billion and projected to grow at a compound annual growth rate (CAGR) of 9.6% from 2024 to 2033 [32]. ACs produced from the abundant PL waste can have a considerable share in this growing demand while offering benefits of low cost, environmental sustainability, and realisation of circular economy [33- 35].

AC production requires dehydration, carbonization, activation, and acid-washing. The dehydration process is typically carried out at a low temperature of roughly 150 ^oC. In an inert environment (N_2, Ar, etc.), carbonization is achieved at high temperatures (600 ^oC - 900 ^oC [34, 36]. Activation can be implemented by either physical (PA) or chemical processes (CA). The PA involves temperatures between 750 and 1000 °C and yields partially oxidised pore formations. On the other hand, CA involves subjecting the the raw materials to chemical agents (such as KOH, K_2CO_3, $ZnCl_2$, H_3PO_4, and $CaCl_2$) and heating them at lower temperatures (550-800 °C). The chemicals intesifies the formation of pores and resulting in a product with a larger surface area [37, 38]. In the final stage phase common to both PA and CA, ash and other residues are eliminated by washing the ACs with dilute acids (e.g., 0.1M HCl).

Numerous studies have been conducted to explore the production of AC from PL, highlighting its potential as a low-cost and abundant precursor for environmental applications. Qiu and Guo [33] investigated the general quality of PL-derived granular AC and confirmed its capacity for organic pollutant removal. Besides this, Guo and Song [34] optimized carbonization conditions to improve benzene adsorption efficiency, demonstrating the significance of thermal control. Similarly, De Lima et al. [35] emphasized the relevance of source material and activation strategy in achieving effective simultaneous removal of heavy metals such as Cu, Cr, and Zn. These works collectively show that PL can serve as an effective base material for AC with promising adsorption properties.

Building on these initial findings, further studies have focused on enhancing PL-derived ACs' structure and surface characteristics through various activation and post-treatment techniques. For instance, Ruiz-Ojeda et al. [39] compared KOH and H_3PO_4 activation methods, finding notable differences in surface area development and pollutant retention. In a series of foundational contributions, Lima and colleagues [40-45] systematically investigated raw and activated chars from broiler and turkey manure, examining how activation temperature and chemical treatment affect porosity, surface functional groups, and heavy metal uptake. Supporting these findings, Klasson et al. [46] confirmed that such activated materials could also be applied to mercury removal from flue gas. These studies validate PL as a feedstock and highlight the flexibility of activation strategies in tailoring material performance.

In recent years, some researchers have pushed the boundaries of traditional adsorption applications by exploring electrochemical and energy-related uses of PL-based AC. For example, Tyagi et al. [36] produced chemically activated carbon with electrocatalytic activity for oxygen reduction reactions, while Pontiroli et al. [47] demonstrated the feasibility of using super-activated biochar in high-performance supercapacitor electrodes. These studies signal a growing interest in expanding the utility of PL-derived carbon materials beyond environmental remediation, although they largely remain at the conceptual or material development stage.

However, despite the growing body of literature, a significant limitation remains: most of these studies have been restricted to laboratory or small pilot-scale conditions. Azargohar et al. [37] and Lima et al. [45] investigated the effect of pyrolysis parameters on material properties in controlled settings. Likewise, Isemin et al. [48] and Ayub et al. [49] examined hydrothermal and gasification-based valorization from a systems analysis perspective without applying industrial-scale implementation. Even optimization-focused studies, such as Yusuff et al. [50], relied on small-scale synthesis and batch testing setups. As a result, the transition from proof-of-concept to scalable, real-world applications remains largely unexplored.

In contrast to these earlier efforts, the present study advances the field by utilizing biochar sourced from a fully operational industrial-scale thermal gasification plant that processes poultry litter. To the best of our knowledge, no prior research has investigated the production of AC from the biochar of industrial-scale real gasification power plants. Thus, this study is novel in that it is, for the first time, the biochar, as a waste of an industrial-scale thermal gasification power plant using PL as fuel, converted into high-value-added AC. There is currently insufficient evidence to support the implementation of such an anticipated AC production route in industry. Moreover, operational hazards of this route remain uncertain. This real-world feedstock, which is typically overlooked in academic investigations, allows for a more realistic assessment of activated carbon production potential and performance. By bridging the gap between laboratory experimentation and industrial relevance, this work contributes essential insights into the feasibility of scaling up PL valorization into commercially viable environmental solutions.

The significance and objectives of this research, therefore, are: (1) to aid the techno-economic competitiveness of industrial gasification-based power plants using PL as fuel by converting their zero-value attributed biochar into commercially important and in-demand AC thus creating added value; (2) determine the activation parameters (temperature, chemical addition, activation time duration and steam flow rate) for converting biochar into best quality AC; (3) investigate the adsorption capacity, isotherms and kinetics of AC for methylene blue (MB) in water; (4) analysis of the technical competitiveness of ACs produced as such in comparison to those reported in the literature. Additionally, possible commercial scale application of industrial scale waste valorisation route proposed by this study can significantly contribute to the attainment of not only zero-waste and circular economy benefits but also a number of the UN Sustainable Development Goals (SDGs: 1 No Poverty, 3 Good Health and Well-being, 6 Clean Water and Sanitation, 7 Affordable and Clean Energy, 8 Decent Work and Economic Growth, 9 Industry, Innovation, and Infrastructure, 11 Sustainable Cities and Communities, 12 Responsible Consumption and Production, 13 Climate Action, 14 Life Below Water, and 15 Life On Land) and aims to address the environmental challenges associated with PL.

MATERIALS AND METHODS

Materials

The methylene blue (MB) (Sigma-Aldric, M9140), NaOH, 99% (Merck, 106498), HCl 37% (Merck, 100317), H_3PO_4, ≥85% (Sigma-Aldrich, 100573) and $ZnCl_2$, ≥98% (Sigma-Aldrich, 208086), deionized water, specific resistivity 18.2 MΩ (Merck, 116754), CO_2 (99.95%) and N_2 (99.99%) from from Elite Gaz Technologies were employed without additional treatment. Biochar samples were obtained from the Bolu Güç Birliği (BGB) field-scale gasification plant in Bolu, Türkiye. This facility gasifies pelletized poultry litter (PL) under optimal conditions to produce syngas and energy.

Methods

Biochar samples collection and characterization

The biochar was collected in 30 kg batches and stored in dark and dry conditions until further processing according to the EPA Field Sampling Procedure and Solid Waste Testing Methods (SW-846) for the physical and chemical characterization of the biochar sample.

Biochar activation process

Chemical activation: Chemical activation agents were employed in varying mass ratios (05:1, 1:1, 2:1) of H_3PO_4 to $ZnCl_2$. The biochar samples were subjected to thermal treatment at 550-800 ^oC under a 100 ml/min N_2 gas flow after being soaked with activating agents.

Physical activation: Biochar samples of 5-10 g were activated physically under CO_2 gas flow of 120 ml/min at 600, 700, and 800 °C.

The duration of activations was 60 minutes with a temperature increase rate of 20 ^oC/min. Following the activation, the mixtures were cooled in N_2, washed with 3 N HCl, and then distilled water until the pH reached neutral. The products were desiccated in an oven at 110°C for 24 hours and packed for the characterisation tests.

Activated carbon characterization

ACs were characterized for functional groups, crystallographic structures, and phases using an energy dispersive X-ray analyser (SEM-EDX, Philips XL 30 SFEG with an EDAX detector), a Fourier transform infrared (FTIR) spectrophotometer (Perkin Elmer 100, USA), and an X-ray diffractometer (Rigaku D/Max 2200 DCI, Tokyo, Japan) with Cu Kα (λ=1.79 ˚A) radiation, respectively. The surface area and pore volumes were calculated with the Micromeritics Gemini VII Surface Area and Porosity Device using N_2.

Adsorption performance investigation

MB adsorption performance of selected ACs was determined according to the ASTM D 3680-98 Standard Method [51]. The adsorption tests were conducted in 250 mL flasks placed in an isothermal water bath shaker (NÜVE ST30) at 250 rpm using 24-h batch mode system with 100 mL various concentration MB solutions, pH, temperature, and mass of AC samples. Following the adsorption process, the samples were filtered with 0.45 µm Whatman PTFE filter and analyzed for the concentration of MB in the solution at 664 nm (the dye maximum absorption wavelength) using a UV-Vis spectrophotometer (Merck Pharo 100, Germany). Each experiment was duplicated under identical conditions. The removal efficiency, Y (%), and the adsorption capacity at equilibrium, q_e (mg/g), of the MB were calculated by applying Eqs. (1) and (2), respectively.

$$Y = \frac{(C_0 - C_e)}{C_0} x\ 100\% \quad (1)$$

$$q_e = \frac{(C_0 - C_e)}{m} x\ V \quad (2)$$

where C_0 is the initial MB concentration (mg/L), C_e is the residual concentration at equilibrium time (mg/L), m is the mass of AC used, and V is the volume of solution

The correlation between the amounts of MB adsorbed onto the ACs and the equilibrium concentration of MB dye in the aqueous phase was evaluated by two different adsorption isotherm models, namely Langmuir and Freundlich:

$$q_e = \frac{q_{max} b C_e}{(1 + b C_e)} \text{ (Langmuir model)} \quad (3)$$

$$q_e = k_F C_e^{1/n} \text{ (Freundlich model)} \quad (4)$$

where q_{max} (mg/g) is the maximum adsorption capacity, b the Langmuir equilibrium constant, k_F (mg/g(L/mg)$^{1/n}$) the adsorption capacity of the adsorbent, and n Freundlich exponent.

To evaluate the adsorption rate, we applied pseudo-first-order (Eq. (5)) and pseudo-second-order (Eq. (6)) kinetic models:

$$\log(q_e - q_t) = \log q_e - \left(\frac{k_1}{2.303}\right) t \quad (5)$$

$$\frac{1}{q_t} = \frac{1}{k_2 q_e^2} + \left(\frac{1}{q_e}\right) t \quad (6)$$

where q_t is the amount of MB adsorbed at time t, k_1 is the rate constant for the pseudo-first order model, and k_2 is the rate constant for the pseudo-second order model.

RESULTS AND DISCUSSION

Biochar Characterization

Physicochemical properties of the biochar sample are summarized in Table 1. Kukwa et al. [2] suggest that the alkaline property (9.65) of biochar can enhance soil pH and regulate cation mobility if applied to acidic soils. Biochar's electrical conductivity (EC) is significantly influenced by the degree to which it has been carbonized, as indicated by its carbon content [52]. Carbon influences the biochar's EC and pH more significantly [53]. As seen from Table 1, our biochar has an alkaline pH, indicating that it contains a high degree of carbon. As evidenced by the 0.73% moisture content in Table 1, our biochar can retain moisture in the soil. These results are consistent with those reported in the literature [2, 54, 55].

Zhou et al. [56] report that the inorganic components of biochar facilitate the adsorption of mineral ions and claim that the biomass template and sorption mechanism influence the ash concentration in biochar. The ash level of 45.2% in our biochar has been found rather suitable for sequestering heavy metals from soil [2]. Song and Gao [23] report that the ash content of biochar produced by pyrolysis from PL increased from 47.9% to 60.8% when the temperature changed from 300 °C to 600 °C. In comparison, the organic carbon content decreased from 38% to 32.5%. Although the

focus of the current article is not to investigate the use of biochar as a soil conditioner, we selected the parameters that should be examined in accordance with the local requirements [57]. It has been found that all the characteristics of biochar were better or equal to those required by the local (Turkish) governmental requirements, except the total Zn content, 1538.3 ppm, being above the required value of 1100 ppm.

Table 1. Physicochemical characteristics of biochar samples

Parameters	Unit	Dry Basis
pH[a]	-	10.1
EC[b]	dS/m	4.2
Moisture[c]	%	0.73
Ash[c]	%	45.16
Volatile matter[d]	%	21.81
Fixed carbon[e]	%	33.03
The higher heating value (HHV)[f]	cal/g	3976
Organic matter[g]	%	56.67
Total nitrogen (N)[h]	%	2.47
Organic nitrogen (N)[ı]	%	1.25
Water soluble phosphorus (P)[j]	%	0.05
Total Copper (Cu)[k]	ppm	118.33
Total Zinc (Zn)[k]	ppm	1538.3
Total Cadmium (Cd)[k]	ppm	<0.005[RL]
Total Lead (Pb)[k]	ppm	76.3
Total Chromium (Cr)[k]	ppm	56.67
Total Nickel (Ni)[k]	ppm	41.3
Total Arsenic (As)[k]	ppm	<0.005[RL]
Total Mercury (Hg)[l]	ppm	<0.005[RL]
Total Sodium (Na)[m]	%	0.816
Total Humic + Fulvic Acid[n]	%	3.42
Total sulphur dioxide[o]	%	1.62
Lime[p]	%	7.02
Chlorine[r]	%	0.583
Specific Gravity	g/cm^3	0.45

Methods: a-1:10 Potentiometric; b-1:10 Aqueous Solution; c- ASTM D 7582; d-ASTM D 7583, e- ASTM D 3172; f- ASTM D 5865; g-70ºC up to constant weight 550ºC Dry burning; h-1965 Bremner; ı-1:10 Potentiometric Kheldahl; j-Annex-3 Article 3.1.6 EN 15959, ICP/AAS [57]; k- TS EN 13650; l- Microwave; m-Annex-3 Article 8.1 ICP/AAS [57]; n- TSI 5869 ISO 5073; o- Annex-3 Article 8.2, Annex-3 Article 8.9 [57]; p- Calcimetric; r- Potentiometric titration/Volhard Method

Activated Carbon Production

Chemical methods

H_3PO_4 activation

To ascertain AC's quality, the relationship between activation agent to biochar weight ratio, activation temperature, surface area, and yield was investigated. The most critical parameter for the processes was found to be the temperature, as shown in Table 2. The data shows that activation commences at 800 ^oC with the lowest H_3PO_4 ratio.

For activation agent to biochar weight ratio 0.5:1, temperature increase from 550 ^oC to 700 °C only boosts the surface area with a very small margin, whilst the temperature increase from 700 ^oC to 800 ^oC, especially for 0.5:1 and 1:1 ratio, causes significant increases (more than tenfold) in the surface area. Therefore, it is understood that activation of PL biochar is greatly enhanced at low agent to biochar ratios (0.5:1 – 1:1) and at higher temperatures (~800 ^oC). The biochar's surface area is increased due to the rapid release of volatile matter at elevated temperatures, which creates numerous pores [58]. In addition, the increased temperatures promote the expansion of pre-existing pores, which augments the total surface area [59].

$ZnCl_2$ activation

Table 2 presents the results of $ZnCl_2$ activation at various temperatures and impregnation rates. As can be noted from Table 2, the mass yields of the AC decrease with increasing temperature. At a 1:1 impregnation ratio, the maximum surface area is achieved at 800 ^oC, measuring 219 m^2/g. Through chemical activation with 3M $ZnCl_2$ at 300 ^oC for 3 hours, Yusuff et al. [50] produced AC with a surface area of 148.05 m^2/g from poultry litter. The values observed by the current work are, thus, in overall agreement with those in existing literature.

Physical activation

Table 2 summarizes the results from activation in CO_2. While an increase in surface area is observed with increasing temperatures, there is a decrease in mass yield. The reason for this is thought to be that CO_2 turns into CO gas at high temperatures, because of the Boudouard reaction (Eq. 7), with the carbon atoms in the biochar structure, reducing the mass of AC but advantageously creating new pores, thus leading to increases in the surface area. Boudroard reaction creates new micropores by removing volatile compounds from the carbon surface and enhancing pore development, leading to further increases in the surface area [60, 61].

$$C + CO_2 \rightarrow 2CO \quad (7)$$

Characterization of Activated Carbons

Table 2 presents the characterization results of selected AC samples. Regardless of the activation method, activations at 800 ^oC yield the highest surface areas. As a result, chemical substances for activation are unnecessary.

Figure 1(a) shows the FT-IR analysis of ACs and biochar samples. It can be deduced from the charts that the presence of aliphatic C-H stretches at 2987.6 cm^{-1} wavelengths, stretching vibrations of alkyne and nitrile groups at 2300-2102 cm^{-1} wavelengths, carbonyl (C=O), alkene (C=C), and amine groups at 1650.9 cm^{-1} wavelengths on the biochar sample surface. In addition, C-O stretching vibrations at wavelengths 1275-1260 cm^{-1} indicate the presence of oxygen-containing groups such as ethers, esters, or alcohols. Likely, asymmetric stretching vibrations of nitro groups (1360-1290 cm^{-1}) and outer plane C-H bending of aromatic rings are also present (700-900 cm^{-1}). Thus, oxygen-containing groups on the AC surface may create chemical interactions between the pollutant and adsorbent during the adsorption process, allowing specific pollutants to bind more strongly to the surface. Similarly, surface functional groups can possibly affect the pore structure; thus, they provide selectivity in pollutant adsorption [62]. Comparison of the spectra of AC and biochar samples suggests that the surface functional groups in the physically activated AC are similar to those of the biochar. At the same time, there is an increase in the surface functional groups of ACs obtained by chemical

activation. As a result of chemical activation, it is seen that aromatic groups (3052.6-3054.8 cm^{-1} band) and functional groups containing more carbonyl groups at 2650-1990-1830 cm^{-1} wavelengths are formed in the material structures in addition to other stresses.

Table 2. Summary of chemical and physical activation results

Sample IDI	Activation Impregnation (g C: g BC)+	Activation temperature (°C)	Mass Yield (%)	BET (m^2/g)
051HPLWAC550	05:1	550	88	24.1
11HPLWAC550	1:1	550	79	25.9
21HPLWAC550	2:1	550	72	29.7
051HPLWAC700	05:1	700	82.5	24.7
11HPLWAC700	1:1	700	78	24.8
21HPLWAC700	2:1	700	68.8	20.7
051HPLWAC800	**05:1**	**800**	**77.3**	**279.6**
11HPLWAC800	1:1	800	78.7	215.7
21HPLWAC800	2:1	800	65.7	18.4
051ZnPLWAC550	05:1	550	98.3	38.7
11ZnPLWAC550	1:1	550	93.3	31.5
21ZnPLWAC550	2:1	550	43.3	63.2
30ZnPLWAC550	%30	550	74.3	45.3
051ZnPLWAC700	05:1	700	54.3	42
11ZnPLWAC700	1:1	700	59.1	42
21ZnPLWAC700	2:1	700	54.3	50.9
30ZnPLWAC700	%30	700	50	31.6
051ZnPLWAC800	05:1	800	36.4	132.7
11ZnPLWAC800	**1:1**	**800**	**41.4**	**219**
21ZnPLWAC800	2:1	800	28.3	N/D*
30ZnPLWAC800	%30	800	24.3	94.1
CPLWAC600	-	600	75.9	22.4
CPLWAC700	-	700	72.5	84.3
CPLWAC800	**-**	**800**	**57.2**	**180.6**

+C: Chemicals (H_3PO_4 or $ZnCl_2$), BC: Biochar; * Not Detectable (below the detection limits)

XRD analyses of the adsorbent samples are shown in Figure 1(b). The phase identification based on XRD patterns was conducted by comparing the observed diffraction peaks with standard reference data from the Joint Committee on Powder Diffraction Standards (JCPDS) database [63]. In the biochar sample, diffraction peaks near 28° and 40° (2θ) indicate the presence of Sylvite (KCl), consistent with JCPDS card No. 00-001-0776 [64]. In addition, the presence of intense peaks at approximately 24°, 26°, 28°, 30°, 31°, and 42° (2θ) suggests the formation of $KClO_4$ crystals [65]. For the CPLWAC800 sample, peaks observed at around 22°, 30°, 32°, 40°, and 45° (2θ) correspond to $KNaCa_2(PO_4)_2$, while the peaks at approximately 42° and 62° (2θ) indicate the formation of MgO, confirmed by JCPDS card No. 00-045-0946 [66, 67]. In the 051HPLWAC800 sample, structural changes due to chemical activation are evident. Peaks at around 27°, 28°, 34°, and 57° (2θ) confirm the presence of potassium zinc phosphate, matching JCPDS card No. 00-025-1455, whereas additional peaks at 19°, 20°, 26°, 27°, 29°, 31°, and 41° (2θ) suggest the formation of the pyrophosphite ($K_2CaP_2O_7$) phase, in agreement with JCPDS card No. 00-033-0973 [68]. The 11ZPLWAC800 sample exhibits peaks of varying intensities at approximately 26°, 28°, 30°, 39°, 47°, 51°, and 56° (2θ), which are attributed to sphalerite and wurtzite crystal phases, consistent with JCPDS card Nos. 00-005-0566 and 00-036-1451, respectively [69, 70]. These assignments reinforce the accuracy of the crystallographic identifications and confirm that the activation methods employed induce distinct mineralogical transformations in the biochar structure.

As expected, the C content by weight of ACs increases from that of the biochar structure (34.3%), with the highest being in 11ZPLWAC800 (75.9%), as shown in the Supplementary Material (Table S1). The other carbon ratios were 54.86% and 44.98% for PLWCAC800 and 051HPLWAC800 samples, respectively. The results showed that oxygen was the other major component on the adsorbent surfaces after carbon. Depending on the activation method, an increase in the P content for the 051HPLWAC800 sample was observed. This confirms that the activation method affects the elemental structure of activated carbon. Although SEM or TEM analyses were not conducted in this study, we acknowledge their

potential to provide valuable morphological insights and recommend their inclusion in future work to further elucidate the structural evolution during activation.

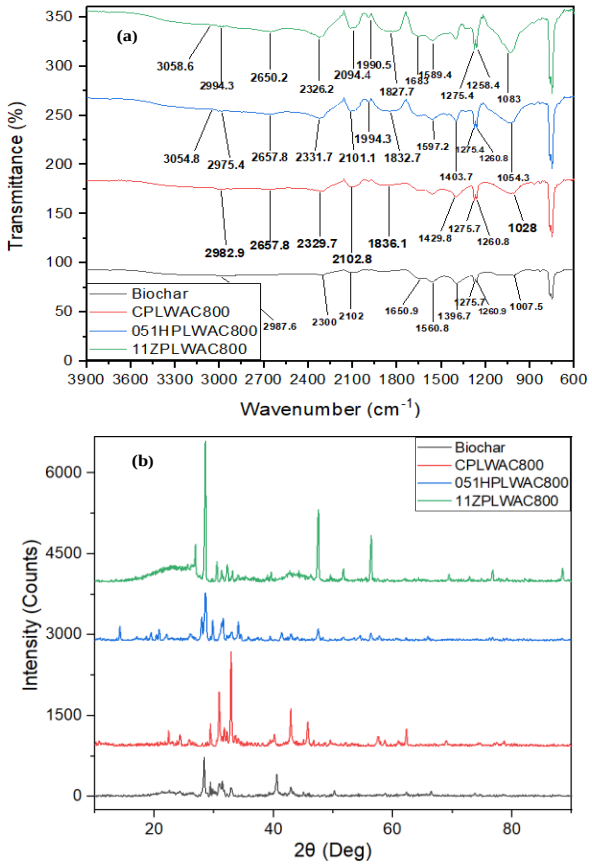

Figure 1. (a) FTIR analysis and (b) XRD analysis of activated carbons and biochar samples

Adsorption of Methylene Blue (MB) by ACs and Biochar

We quantified the performance of our ACs for water treatment, which was represented by MB solutions. We changed the initial concentration of the pollutant (MB), the adsorbent (AC) dose, the medium pH, and the temperature, to determine favourable conditions. Through analysis of experimental results and fitting of isotherm and kinetic models, we alluded the mechanism of the adsorption process. Additionally, we conducted a thermodynamic analysis to examine the chemistry of the reaction.

Effect of initial MB concentration

Figure 2a illustrates that the most favourable adsorption capacity of each sorbent (ACs and biochar) is achieved at a distinct concentration, and the adsorption capacities of the samples exhibit substantial disparities. It is evident from Figure 2a that the MB adsorption capacity of biochar exceeds that of some ACs, namely the 051HPLWAC800 and 11ZPLWAC800 samples, which were obtained through physical activation. A high adsorption rate characterised the initial phase of the treatment due to numerous functional groups and vacant sites on the ACs and biochar's surfaces, which may have formed hydrogen bonds or interacted electrostatically with dye molecules. However, the uptake of these sites decreased over time, resulting in a saturation of the curve [71]. As the initial concentration increases, the adsorbed quantity increases while the removal efficiency decreases for all ACs and biochar samples. It is observed that MB with an initial concentration of 50 mg/L is almost completely adsorbed by two activated carbons (CPLWAC800 and 11ZPLWAC800). The decrease in the absorption percentage of dyes (pollutants) results from the overabundance of pollutants that surpasses the number of available adsorption sites [72]. The depicted results indicate that the adsorbents contain a specific number of active sites for the adsorption of MB dye. This suggests numerous underutilized active sites, as the number of active sites for the adsorbent of the dye molecule exceeded the number of dye molecules. This results in a reduction in the adsorption capacity [73]. We determined the most favourable initial MB concentration to be 75 mg/l from the results. While investigating the effect of other operational parameters, we fixed the level of the MB initial concentration at this value.

The effect of adsorbent quantity

Figure 2b illustrates the effect of adsorbent quantity, ranging from 0.5 to 4 g/100 mL on the MB adsorption. As being apparent from the curves, the adsorption capacity of all AC samples decreases as the adsorbent amount increases whereas the absorption capacity of biochar sample does not change significantly. This decrease was attributed to the increased adsorption surface area and the presence of a greater number of active voids or groups of functional surfaces that were involved in the adsorption mechanisms [74, 75]. It is imperative not to waste the adsorbent material by using enough quantity that is not much beyond the equilibrium [76] depending on the mass transfer rate at breakthrough. While the efficiency of pollutant removal increases as the quantity of adsorbent increases, the use of an excessive amount of adsorbent is not cost-effective. In general, an increase in the adsorbent dosage results in a greater number of active sites or surface area for the interaction between the dyes and powdered activated carbons [77].

The percentage of the dyes that are removed is increased by the availability. The adsorbents demonstrated satisfactory performance for MB as per the literature [14, 78], even when the adsorbent dosage was minimal. This suggests the MB has sufficient active sites to react and adsorb effectively. Although the adsorption capacity appears to be high when the adsorbent dosage is reduced, the time-dependent pollutant removal efficiencies are relatively lower. Consequently, the adsorbent dosage that is the most effective within the range investigated in the experiments is inferred to be 1 g/L, and the research was subsequently continued at this dosage.

The effect of medium pH

The net charge on the surface of both the adsorbent and the adsorbate is altered because of the functional groups' protonation and deprotonation in response to the pH solution variation [79]. This significantly impacts the dye's adsorption. Typically, the medium pH is influenced by the electrostatic interaction with the adsorption surface of the ions in the reaction mixture [80]. The ionization of the adsorbate and the surface charge of the adsorbent are both influenced by the medium pH. Also, the adsorption efficacy in aqueous solutions is influenced by other factors such as hydrogen bonds, hydrophobic interaction, π-π interaction, and n-π interaction [81]. Figure 2c illustrates the MB adsorption performance of the adsorbents as a function of the medium pH. It is evident from Figure 4c that the CPLWAC800 (physical activation) sample exhibits the highest adsorption capacity,

but no changes with the medium pH. Regarding other adsorbent, they demonstrate varying adsorption capacities with the medium pH. It is known that the medium pH level can impact both the chemical composition of the solution and the affinity of the adsorbents for surface binding sites [82]. This observed behaviour suggests that AC samples exhibit varying surface charges at different pH levels. MB is a type of cationic dye that reacts with the surface charges of the adsorbent under varying pH conditions. As expected, the cationic properties of the MB dye resulted in exceptional adsorption in a basic medium. The decreased H^+ charges in the medium as the pH increased leads to a reduction in the competition between positive ions and dye molecules, thus to more adsorption of MB. Electrostatic interactions cause cationic species (i.e. MB) to absorb on the surface of negatively charged adsorbents ($pH>pH_{pzc}$) [80]. While direct measurements of zeta potential and pH_{pzc} were not performed in this study, these findings support the proposed electrostatic interaction mechanism. Future work will include direct surface charge analysis through zeta potential and pHpzc measurements to validate these inferences and deepen understanding of the adsorbent–adsorbate interactions.

The effect of medium temperature

The medium temperature, influencing the solid-solute interface and the mobility and solubility of contaminants, was another critical parameter that can directly influence the adsorption of contaminants [83]. As illustrated in Figure 2d, the adsorption capacity of the biochar and that of 051HPLWAC800 increase with temperature, while those of CPLWAC800 and 11ZPLWAC800 were not significantly influenced and are comparable at all temperatures. The CPLWAC800 sample exhibits the highest adsorption capacity. Furthermore, it is apparent that the ACs obtained through phosphoric acid activation (051HPLWAC800) exhibit a lower adsorption capacity in comparison to that of biochar under almost all investigated conditions. However, the adsorption capacity is approximately 1.3 times higher than biochar for AC activated in zinc chloride. The adsorption of MB on activated carbon involves mainly two types of interaction, namely electrostatic interactions between surface phosphoric and oxygenated groups with MB and hydrogen bonding between surface hydroxyl groups with MB [84].

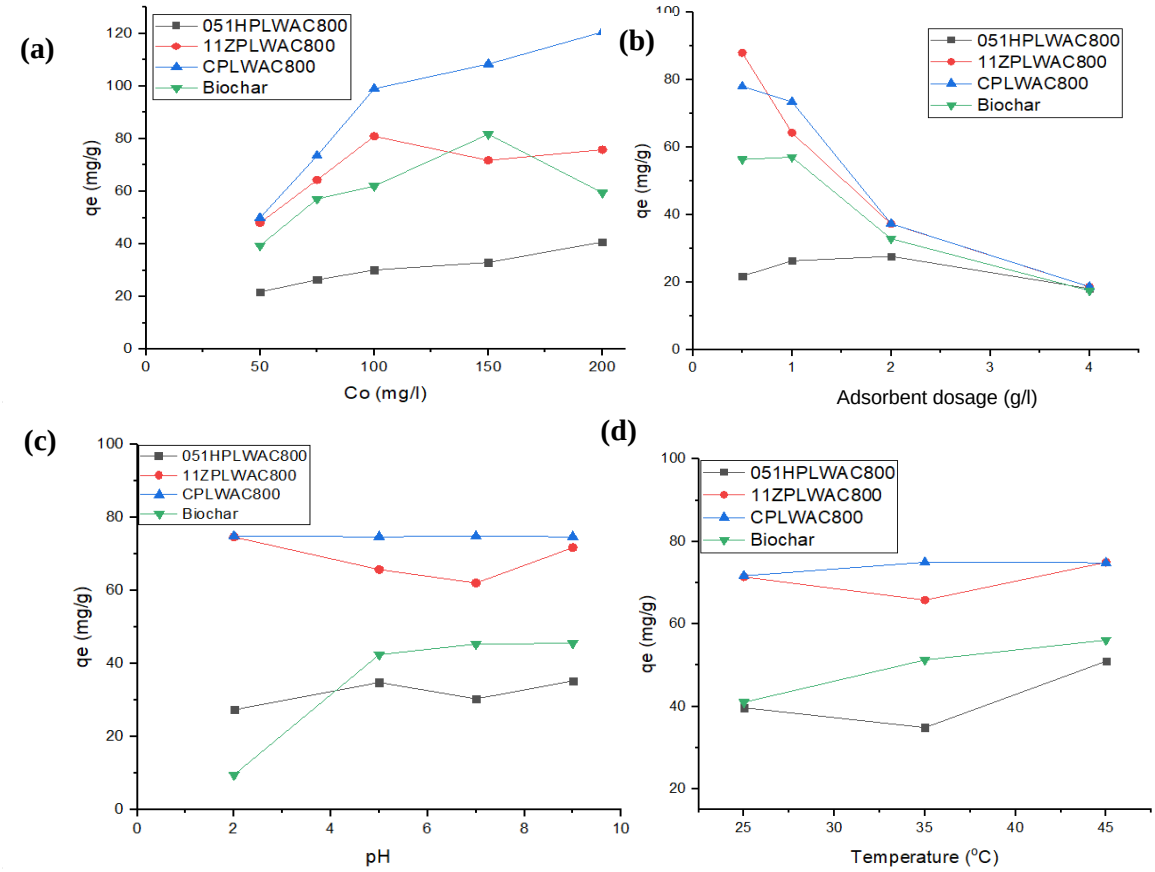

Figure 2. Factors affecting adsorption; a) Initial MB concentration (25 °C, pH 5.5, 1 g/L adsorbent dosage), b) Adsorbent dosage (25 °C, pH 5.5, 75 mg/L cons.), c) pH (25 °C, 1 g/L adsorbent dosage, 75 mg/L cons.), d) Temperature (pH 5.5, 1 g/L adsorbent dosage, 75 mg/L cons.)

Adsorption Isotherm Studies

An isotherm delineates the equilibrium relationship between the adsorbate concentrations in the liquid phase and the amount of adsorption in both the liquid and solid phases at a certain temperature [74]. Following identifying the most favourable conditions for adsorption performance within the range we investigated in the present work, we conducted additional tests to develop adsorption isotherms. The results are presented in Figure 3, as Langmuir and Freundlich isotherm models at 25 °C and pH 5.5 for different MB concentrations, fixed AC dosages, and biochar at 1 g/l adsorbent. The values of the crucial parameters of the isotherm models are given in the Supplementary Material (Table S2). From the linear Langmuir fit results, the maximum MB adsorption capacity (q_{max}) of AC samples of 051HPLW,

11ZPLW, and CPLW reached up to 48.6, 75.5, and 119.3 mg/g, respectively, while the maximum adsorption capacity of biochar reached up to 62.2 mg/g. The linear Langmuir model fits well with the experimental data having R^2 values of 0.97, 0.99, 0.99 and 0.97 for 051HPLW, 11ZPLW, CPLW and biochar, respectively compared to Freundlich models where the R^2 values remained in a range of 0.47-0.96. The values of n for each ACs and biochar type in Freundlich were 1, which indicates that adsorption conditions were favourable as given in Table S2.

A very good fit of the Langmuir isotherm model indicates that the MB adsorbs on ACs and biochar as a single-layer. This is consistent with prior research that also reported the adsorption of MB using the Langmuir isotherm [82, 85]. The CPLWAC800 sample (physical activation in CO_2), exhibited the highest adsorption capacity (119.3 mg/g). The homogeneity of the surface sites on ACs and biochar samples and the typical monolayer adsorption of MB on ACs and biochar were demonstrated by the perfect fit of adsorption data with the Langmuir isotherm model [85].

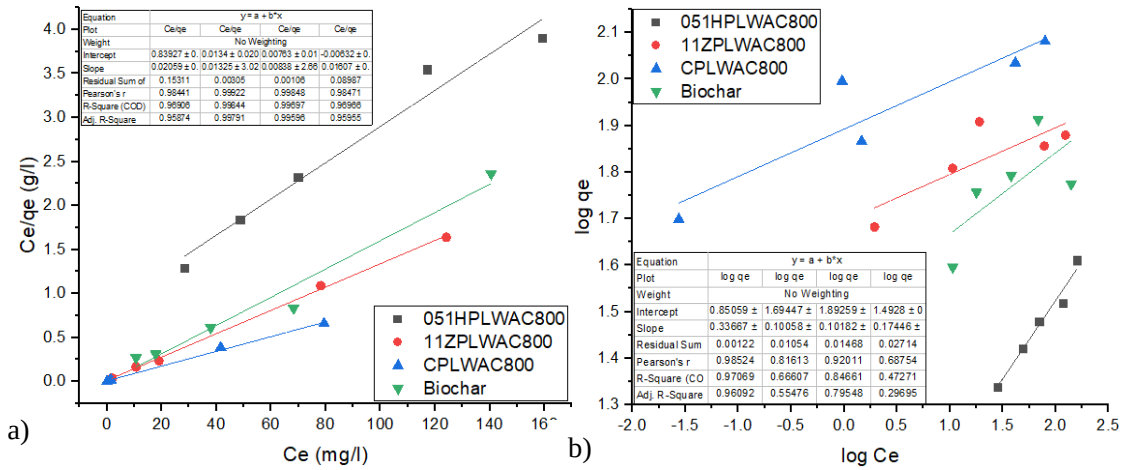

Figure 3. Adsorption isotherm models (25 oC, pH 5.5, 1 g/l adsorbent dosage); a) Langmuir Isotherm, b) Freundlich Isotherm

Table 3. Activation types, BET and adsorption capacities of various adsorbents for MB from the literature in comparison to those produced in current work

AC Feedstock	Activation type	BET (m^2/g)	Adsorption capacity (mg/g)	Reference
Torrefied bamboo biochar	KOH	366	83.3	[30]
Sludge-adsorbents from palm oil mill effluent	$ZnCl_2$	29.2	22.4	[86]
	KOH	79.4	23.5	
Pine apple waste biomass	$ZnCl_2$	284.2	40	[87]
Poultry wastes digestate biochar	HNO_3	-	101.72	[88]
	KOH	-	58.67	
Commercial activated carbon	-	938	22.3	[89]
Corn husk waste	HNO_3	12.65	41.06	[90]
Coconut coir dust carbon	$ZnCl_2$	1884	14.4	[91]
Activated sewage sludge	H_2SO_4	390	194	[92]
Rice husk carbon	$ZnCl_2$	181	9.73	[93]
Poultry litter biochar	H_3PO_4	279.6	48.6	This study
	$ZnCl_2$	219	75.5	
	CO_2	180.6	119.3	

In Table 3, the removal of MB by a variety of adsorbents from the relevant literature in comparison to our results is summarized. It is important to realize that the adsorption capacity of specific adsorbents for MB depends on the medium pH, presence, properties of surface functional groups, and pore morphologies [86]. Our results reveal that the adsorption capacity of biochar is competitive with the biomass-based ACs (Table 3). Our study demonstrates that physically activated AC in CO_2 from poultry litter biochar has a superior adsorption capacity of 119.3 mg/g compared to other materials, such as corn husk waste at 41.06 mg/g and torrefied bamboo biochar at 83.3 mg/g. We believe that the primary cause for this is high-level pore formation in the gasification process, which is characterized by temperatures of 900 °C and higher. Additionally, the pores are susceptible to clogging with tar, a problem in the pyrolysis process (which occurs at approximately 500 °C) but not in the gasification process. The outstanding efficiency of ACs

produced in our current work proves that producing ACs from biochar of gasification-based power plants using broiler waste as fuel is a promising direction for additional future studies and practical use in industry.

Adsorption kinetic studies

Pseudo-first order (PFO) and pseudo-second order (PSO) models have been suggested to elucidate how MB may be adsorbed on ACs and biochar. The rate-controlling stages in the adsorption process were investigated using both the PFO and PSO models. The data's applicability was quantified using correlation coefficients (R^2) [87]. We investigated the adsorption rate of AC and biochar samples at 25, 35 and 45 ^oC, pH 5.5 for 100 ml MB solution with a concentration of 75 mg/l using 1 g/l adsorbent and determined the suitability of adsorption to pseudo-first order and pseudo-second order kinetic models. Figures 4 and 5 show the results obtained for the pseudo-first-order and pseudo-second-order kinetic modelling of AC and biochar samples, respectively. The critical parameters derived from these kinetic models are given in the Supplementary Material (Table S3).

The high correlation coefficients observed from the model fits suggest that all samples are consistent with the second-order reaction kinetics model. The determination coefficient (R^2) derived from the PSO model was found to be higher than that of the PFO model. The results obtained in the study are consistent with the literature in that dyestuff adsorption is typically accounted for by second-order reaction kinetics [94]. The CPLWAC800 exhibits stable adsorption behaviour in all adsorption conditions, as indicated by the values in Table 1, especially by the highest correlation coefficient (0.999). The results indicate that physically activated AC is suitable for use as an adsorbent material.

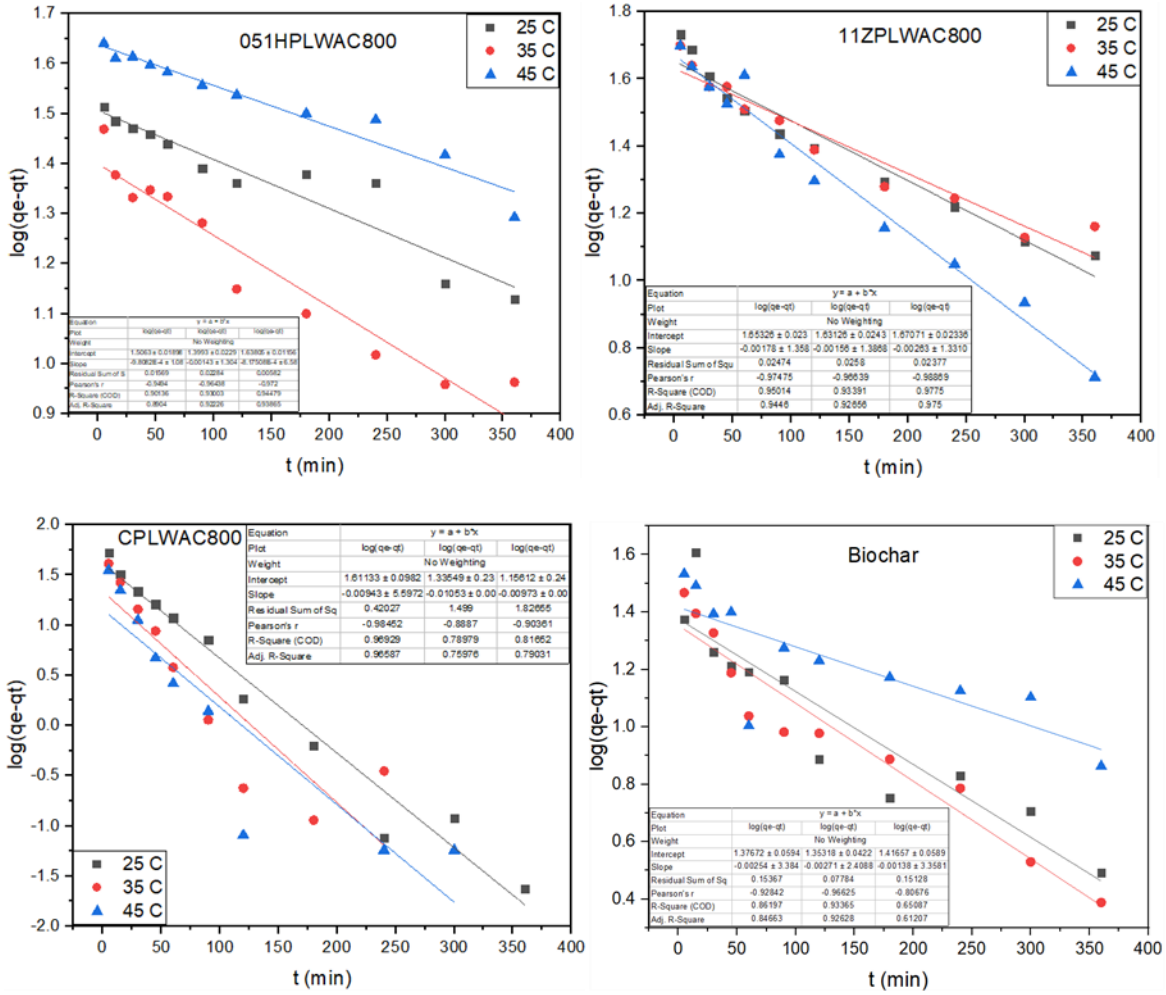

Figure 4. Pseudo First Order Kinetic Model

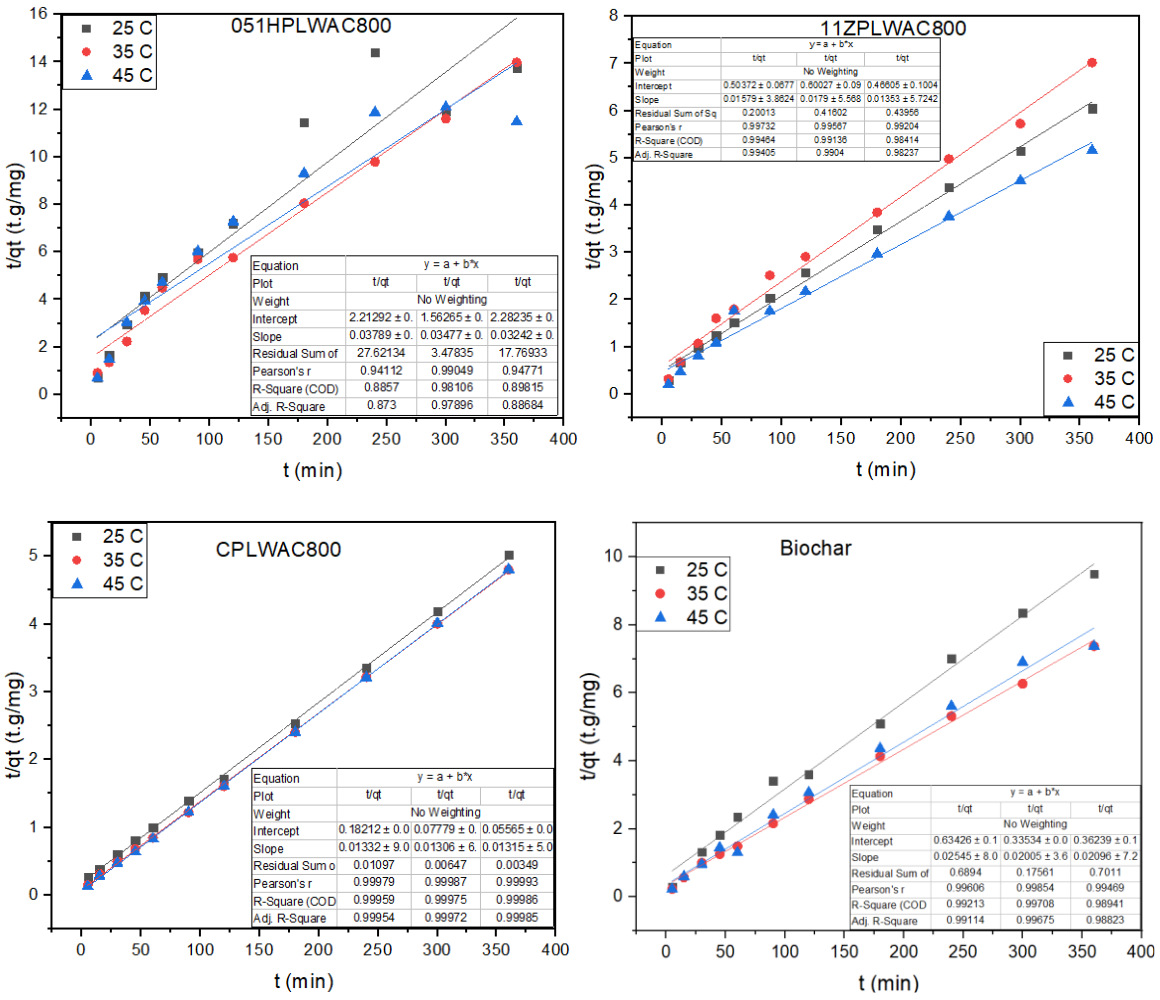

Figure 5. Pseudo Second Order Kinetic Model

CONCLUSIONS

Current work, investigated for the first time the production of activated carbons (ACs) derived from the waste biochar of an industrial-scale thermal gasification of poultry litter (an agricultural waste) characterized them with regards to important properties of ACs, and their potential for being used as an adsorbent for the removal of MB dye from aqueous solution. The main conclusions from the work are:

1. ACs, especially CPLWAC800 with an adsorption capacity of 119.3 mg/g, was effective for the removal of MB from aqueous solution.
2. The surface areas of the AC obtained by chemical activation varied in the range of 219-280 m^2/g, while the maximum surface area of the physically activated AC in CO_2 gas at 600, 700 and 800 °C temperature conditions, and were 181 m^2/g.
3. Although the surface areas of the ACs produced by physical and chemical activation are quite low compared to commercial ACs (400-1500 m^2/g), they agree with the surface areas of ACs obtained by physical and chemical activation from PL in the literature (148.05-450 m^2/g).
4. The initial concentration, treatment temperature, medium pH, and adsorbent dosage had influence on the amount of pollutant dye adsorbed.
5. The optimal adsorption parameters for each adsorbent are as follows: 051HPLWAC800 for a 200 mg/l initial concentration, 2 g/l adsorbent dosage, pH 5, and 45 °C temperature; 11ZPLWAC800 for a 100 mg/l initial concentration, 0.5 g/l adsorbent dosage, pH 2, and 45 °C temperature; CPLWAC800 for a 200 mg/l initial concentration, 0.5 g/l adsorbent dosage, pH 5, and 35 °C temperature; and 150 mg/l initial concentration, 1 g/l adsorbent dosage, pH 9, and 45 °C temperature for biochar.
6. The Langmuir isotherm model was well-fitted by the equilibrium data, which suggested the formation of a monolayer. The prepared adsorbent exhibited a maximal adsorption capacity of 48.6, 75.5, and 119.3 mg/g for H_3PO_4, $ZnCl_2$, and CO_2 at 25°C, respectively.
7. The rate of adsorption was determined to be in accordance with pseudo-second-order kinetics, as indicated by the highest correlation coefficient.
8. The application of AC derived from PL in water treatment for dye (MB) removal would not present any additional hazardous contaminations.
9. Although reusability tests were not performed in the present study, future work will investigate the regeneration efficiency of the produced activated carbons using standard approaches such as mild acid/base washing or thermal desorption, as commonly employed in the literature for similar materials.

10. Finally, production of AC from poultry litter biochar as a raw material is a feasible method for value-added recycling of organic waste.

DATA AVAILABILITY STATEMENT

The authors confirm that the data that supports the findings of this study are available within the article. Raw data that support the finding of this study are available from the corresponding author, upon reasonable request.

CONFLICT OF INTEREST

The author declares that there is no conflict of interest with any individual, institution, or organization in the preparation, evaluation, or publication of this study.

USE OF AI FOR WRITING ASSISTANCE

Not declared.

ETHICS

There are no ethical issues with the publication of this manuscript.

REFERENCES

[1]. OECD, "Meat consumption (indicator)," 2024. [Online]. Available: https://www.oecd.org/en/data/indicators/meat-consumption.html. [Accessed: 13 Oct. 2024].

[2]. R. E. Kukwa, D. T. Kukwa, and S. S. Barnabas, "Reclamation of poultry litter for the production of biochar," International Journal of Recycling of Organic Waste in Agriculture, Vol. 12(Special Issue), pp. 147–158, 2023. https://doi.org/10.30486/ijrowa.2023.1960315.1490.

[3]. FAO, "Meat and meat products," 2023. [Online]. Available: https://www.fao.org/3/cb9427en/cb9427en_meat.pdf. [Accessed: 29 Aug. 2023].

[4]. S. Katuwal, N.-A.-S. Rafsan, A. J. Ashworth, and P. Kolar, "Poultry litter physiochemical characterization based on production conditions for circular systems," BioResources, Vol. 18(2), pp. 3961–3977, 2023. https://doi.org/10.15376/biores.18.2.3961-3977.

[5]. İ. Acar, "Utilization potential of poultry litter ash as phosphorus-based fertilizer," Environmental Research and Technology, Vol. 6(2), pp. 102–107, 2023. https://doi.org/10.35208/ert.1243895.

[6]. A. J. Ashworth, J. P. Chastain, and P. A. Moore Jr., "Nutrient characteristics of poultry manure and litter," in ASA Special Publication, Vol. 67, pp. 63–87, 2020. https://doi.org/10.2134/asaspecpub67.c5.

[7]. EU, "The EU poultry meat and egg sector," 2019. [Online]. Available: https://www.europarl.europa.eu/RegData/etudes/IDAN/2019/644195/EPRS_IDA(2019)644195_EN.pdf. [Accessed: 11 Feb. 2025].

[8]. B. L. Masocha and O. Dikinya, "The role of poultry litter and its biochar on soil fertility and Jatropha curcas L. growth on sandy-loam soil," Applied Sciences, Vol. 12(23), p. 12294, 2022. https://doi.org/10.3390/app122312294.

[9]. N. S. Bolan, A. A. Szogi, T. Chuasavathi, B. Seshadri, M. J. Rothrock, and P. Panneerselvam, "Uses and management of poultry litter," World's Poultry Science Journal, Vol. 66(4), pp. 673–698, 2010. https://doi.org/10.1017/s0043933910000656.

[10]. D. Castillo, J. C. Cruz, D. L. Trejo-Arroyo, E. M. Muzquiz, Z. Zarhri, M. P. Gurrola, and R. E. Vega-Azamar, "Characterization of poultry litter ashes as a supplementary cementitious material," Case Studies in Construction Materials, Vol. 17, p. e01278, 2022. https://doi.org/10.1016/j.cscm.2022.e01278.

[11]. H. K. Jeswani, A. Whiting, A. Martin, and A. Azapagic, "Environmental and economic sustainability of poultry litter gasification for electricity and heat generation," Waste Management, Vol. 95, pp. 182–191, 2019. https://doi.org/10.1016/j.wasman.2019.05.053.

[12]. G. Gržinić, A. Piotrowicz-Cieślak, A. Klimkowicz-Pawlas, R. L. Górny, A. Ławniczek-Wałczyk, L. Piechowicz, and L. Wolska, "Intensive poultry farming: A review of the impact on the environment and human health," Science of the Total Environment, Vol. 858, p. 160014, 2023. https://doi.org/10.1016/j.scitotenv.2022.160014.

[13]. Y. Yang, X. Qian, S. O. Alamu, K. Brown, S. W. Lee, and D. H. Kang, "Qualities and quantities of poultry litter biochar characterization and investigation," Energies, Vol. 17(12), p. 2885, 2024. https://doi.org/10.3390/en17122885.

[14]. K. K. Pandey, S. Koley, B. K. Ojha, N. Kurechiya, S. Singh, and A. Singh, "In ovo feeding: Viewpoints on the current status, application and prospect in poultry," Indian Journal of Animal Research, Vol. 60(2), 2021. https://doi.org/10.36062/ijah.2021.04021.

[15]. J. A. Antonangelo and H. Zhang, "The use of biochar as a soil amendment to reduce potentially toxic metals (PTMs) phytoavailability," in Applications of Biochar for Environmental Safety, p. 177, 2020. https://doi.org/10.5772/intechopen.92611.

[16]. M. Guo, M. Labreveux, and W. Song, "Nutrient release from bisulfate-amended phytase-diet poultry litter under simulated weathering conditions," Waste Management, Vol. 29(7), pp. 2151–2159, 2009. https://doi.org/10.1016/j.wasman.2009.02.012.

[17]. K. Y. Chan, L. Van Zwieten, I. Meszaros, A. Downie, and S. Joseph, "Using poultry litter biochars as soil amendments," Soil Research, Vol. 46(5), pp. 437–444, 2008. https://doi.org/10.1071/SR08036.

[18]. K. Draper and T. Tomlinson, "Poultry litter biochar—a US perspective," International Biochar Initiative, Vol. 6, 2012.

[19]. S. Yu, J. Park, M. Kim, C. Ryu, and J. Park, "Characterization of biochar and by-products from slow pyrolysis of hinoki cypress," Bioresource Technology Reports, Vol. 6, pp. 217–222, 2019. https://doi.org/10.1016/j.biteb.2019.03.009.

[20]. A. Er and S. Özdemir, "Tavuk gübresi ve tarımsal atıkların biyoyakıt karakterlerinin incelenmesi," Sakarya Üniversitesi Fen Bilimleri Enstitüsü Dergisi, Vol. 22(2), pp. 489–494, 2018. https://doi.org/10.16984/saufenbilder.305595.

[21]. Y. Yi, Z. Huang, B. Lu, J. Xian, E. P. Tsang, W. Cheng, and Z. Fang, "Magnetic biochar for environmental remediation: A review," Bioresource Technology, Vol. 298, p. 122468, 2020. https://doi.org/10.1016/j.biortech.2019.122468.

[22]. S. Cheng, T. Chen, W. Xu, J. Huang, S. Jiang, and B. Yan, "Application research of biochar for the remediation of soil heavy metals contamination: a review," Molecules, Vol. 25(14), p. 3167, 2020. https://doi.org/10.3390/molecules25143167.

[23]. W. Song and M. Guo, "Quality variations of poultry litter biochar generated at different pyrolysis temperatures," Journal of Analytical and Applied Pyrolysis, Vol. 94, pp. 138–145, 2012. https://doi.org/10.1016/j.jaap.2011.11.018.

[24]. N. Khan, I. Clark, M. A. Sánchez-Monedero, S. Shea, S. Meier, F. Qi, R. S. Kookana, and N. Bolan, "Physical and

chemical properties of biochars co-composted with biowastes and incubated with a chicken litter compost," Chemosphere, Vol. 142, pp. 14–23, 2016. https://doi.org/10.1016/j.chemosphere.2015.05.065.

[25]. M. Zolfi Bavariani, A. Ronaghi, and R. Ghasemi, "Influence of pyrolysis temperatures on FTIR analysis, nutrient bioavailability, and agricultural use of poultry manure biochars," Communications in Soil Science and Plant Analysis, Vol. 50(4), pp. 402–411, 2019. https://doi.org/10.1080/00103624.2018.1563101.

[26]. P. Q. Thang, K. Jitae, B. L. Giang, N. M. Viet, and P. T. Huong, "Potential application of chicken manure biochar towards toxic phenol and 2,4-dinitrophenol in wastewaters," Journal of Environmental Management, Vol. 251, p. 109556, 2019. https://doi.org/10.1016/j.jenvman.2019.109556.

[27]. G. Duran-Jimenez, J. Rodriguez, L. Stevens, S. Altarawneh, A. Batchelor, L. Jiang, and C. Dodds, "Single-step preparation of activated carbons from pine wood, olive stones and nutshells by KOH and microwaves: Influence of ultra-microporous for high CO2 capture," Chemical Engineering Journal, p. 156135, 2024. https://doi.org/10.1016/j.cej.2024.156135.

[28]. J. B. Njewa, E. Vunain, and T. Biswick, "Synthesis and characterization of activated carbons prepared from agro-wastes by chemical activation," Journal of Chemistry, Vol. 2022, p. 9975444, 2021. https://doi.org/10.1155/2022/9975444.

[29]. T. Mori, S. Iwamura, I. Ogino, and S. R. Mukai, "Cost-effective synthesis of activated carbons with high surface areas for electrodes of non-aqueous electric double layer capacitors," Separation and Purification Technology, Vol. 214, pp. 174–180, 2019. https://doi.org/10.1016/j.seppur.2018.04.022.

[30]. I. U. Bakara, M. D. Nurhafizah, N. Abdullah, O. O. Akinnawo, and A. Ul-Hamid, "Investigation of kinetics and thermodynamics of methylene blue dye adsorption using activated carbon derived from bamboo biomass," Inorganic Chemistry Communications, p. 112609, 2024. https://doi.org/10.1016/j.inoche.2024.112609.

[31]. Global Trade, "Activated carbon price in United States hits new record of $6,401 per ton," 2023. [Online]. Available: https://www.globaltrademag.com/activated-carbon-price-in-united-states-hits-new-record-of-6401-per-ton/. [Accessed: 13 Oct. 2024].

[32]. Precedence Research, "Activated carbon market size, share, and trends 2024 to 2033," 2024. [Online]. Available: https://www.precedenceresearch.com/activated-carbon-market. [Accessed: 13 Oct. 2024].

[33]. G. Qiu and M. Guo, "Quality of poultry litter-derived granular activated carbon," Bioresource Technology, Vol. 101, pp. 379–386, 2010. https://doi.org/10.1016/j.biortech.2009.07.050.

[34]. M. Guo and W. Song, "Converting poultry litter to activated carbon: optimal carbonization conditions and product sorption for benzene," Environmental Technology, Vol. 32(15), pp. 1789–1798, 2011. https://doi.org/10.1080/09593330.2011.556149.

[35]. L. S. De Lima, S. P. Quináia, F. L. Melquiades, G. E. de Biasi, and J. R. Garcia, "Characterization of activated carbons from different sources and the simultaneous adsorption of Cu, Cr, and Zn from metallurgic effluent," Separation and Purification Technology, Vol. 122, pp. 421–430, 2014. https://doi.org/10.1016/j.seppur.2013.11.034.

[36]. A. Tyagi, S. Banerjee, S. Singh, and K. K. Kar, "Biowaste derived activated carbon electrocatalyst for oxygen reduction reaction: Effect of chemical activation," International Journal of Hydrogen Energy, Vol. 45, pp. 16930–16943, 2020. https://doi.org/10.1016/j.ijhydene.2019.06.195.

[37]. R. Azargohar, S. Nanda, J. A. Kozinski, A. K. Dalai, and R. Sutarto, "Effects of temperature on the physicochemical characteristics of fast pyrolysis bio-chars derived from Canadian waste biomass," Fuel, Vol. 125, pp. 90–100, 2014. https://doi.org/10.1016/j.fuel.2014.01.083.

[38]. G. Sharma, S. Sharma, A. Kumar, C. W. Lai, M. Naushad, Shehnaz, and F. J. Stadler, "Activated carbon as superadsorbent and sustainable material for diverse applications," Adsorption Science and Technology, p. 4184809, 2022. https://doi.org/10.1155/2022/4184809.

[39]. M. Ruiz-Ojeda, L. Fonseca, and E. Amado-González, "Optimization of activated carbon production from chicken manure by chemical activation with KOH and H3PO4," Chemical Engineering Transactions, Vol. 50, pp. 115–120, 2016. https://doi.org/10.3303/CET1650020.

[40]. I. M. Lima and W. E. Marshall, "Granular activated carbons from broiler manure: physical, chemical and adsorptive properties," Bioresource Technology, Vol. 96(6), pp. 699–706, 2005.https://doi.org/10.1016/j.biortech.2004.06.021.

[41]. I. M. Lima and W. E. Marshall, "Utilization of turkey manure as granular activated carbon: physical, chemical and adsorptive properties," Waste Management, Vol. 25, pp. 726–732, 2005. https://doi.org/10.1016/j.wasman.2004.12.019.

[42]. I. M. Lima, A. A. Boateng, and K. T. Klasson, "Pyrolysis of broiler manure: char and product gas characterization," Industrial and Engineering Chemistry Research, Vol. 48, pp. 1292–1297, 2009. https://doi.org/10.1021/ie800989s.

[43]. I. M. Lima, D. L. Boykin, K. T. Klasson, and M. Uchimiya, "Influence of post-treatment strategies on the properties of activated chars from broiler manure," Chemosphere, Vol. 95, pp. 96–104, 2014. https://doi.org/10.1016/j.chemosphere.2013.08.027.

[44]. I. M. Lima, K. S. Ro, G. B. Reddy, D. L. Boykin, and K. T. Klasson, "Efficacy of chicken litter and wood biochars and their activated counterparts in heavy metal clean up from wastewater," Agriculture, Vol. 5, pp. 806–825, 2015. https://doi.org/10.3390/agriculture5030806.

[45]. I. M. Lima, K. T. Klasson, and M. Uchimiya, "Selective release of inorganic constituents in broiler manure biochars under different post-activation treatments," Journal of Residuals Science and Technology, Vol. 13(1), pp. 37–48, 2016. https://doi.org/10.12783/issn.1544-8053/13/1/6.

[46]. K. T. Klasson, I. M. Lima, L. L. Boihem Jr., and L. H. Wartelle, "Feasibility of mercury removal from simulated flue gas by activated chars made from poultry manures," Journal of Environmental Management, Vol. 91(12), pp. 2466–2470, 2010. https://doi.org/10.1016/j.jenvman.2010.06.028.

[47]. D. Pontiroli, S. Scaravonati, G. Magnani, L. Fornasini, D. Bersani, G. Bertoni, C. Milanese, A. Girella, F. Ridi, R. Verucchi, L. Mantovani, A. Malcevschi, and M. Riccò, "Super-activated biochar from poultry litter for high-performance supercapacitors," Microporous and Mesoporous Materials, Vol. 285, pp. 161–169, 2019. https://doi.org/10.1016/j.micromeso.2019.05.002.

[48]. R. Isemin, N. Muratova, S. Kuzmin, D. Klimov, V. Kokh-Tatarenko, A. Mikhalev, and B. Rogge, "Characteristics of

hydrochar and liquid products obtained by hydrothermal carbonization and wet torrefaction of poultry litter in mixture with wood sawdust," Processes, Vol. 9(11), p. 2082, 2021. https://doi.org/10.3390/pr9112082.

[49]. Y. Ayub, J. Zhou, and J. Ren, "Critical reviews of hydrothermal gasification for poultry litter valorization: Process yield, economic viability, environmental sustainability and safety," Journal of Cleaner Production, Vol. 415, p. 137876, 2023. https://doi.org/10.1016/j.jclepro.2023.137876.

[50]. A. S. Yusuff, O. A. Ajayi, and L. T. Popoola, "Application of Taguchi design approach to parametric optimization of adsorption of crystal violet dye by activated carbon from poultry litter," Scientific African, Vol. 13, p. e00850, 2021. https://doi.org/10.1016/j.sciaf.2021.e00850.

[51]. ASTM D 3680-98, "Standard method," 2003. [Online]. Available: https://cdn.standards.iteh.ai/samples/28716/d05cd48abb9b4042a907fba775f5554f/ASTM-D3080-03.pdf. [Accessed: 12 Oct. 2024].

[52]. A. A. Almutairi, M. Ahmad, M. I. Rafique, and M. I. Al-Wabel, "Variations in composition and stability of biochars derived from different feedstock types at varying pyrolysis temperature," Journal of the Saudi Society of Agricultural Sciences, Vol. 22(1), pp. 25–34, 2022. https://doi.org/10.1016/j.jssas.2022.05.005.

[53]. H. Singh, B. K. Northup, C. W. Rice, et al., "Biochar applications influence soil physical and chemical properties, microbial diversity, and crop productivity: a meta-analysis," Biochar, Vol. 4(8), 2022. https://doi.org/10.1007/s42773-022-00138-1.

[54]. Y. Aktaş, S. S. Ok, and S. C. Çetin, "Influence of poultry litter biochar on some properties and carbon mineralization in acidic soil," Agricultural Engineering, Vol. 377, pp. 33–44, 2023. https://doi.org/10.33724/zm.1156809.

[55]. L. Chaves, J. Fernandes, J. Mendes, G. Tito, H. Guerra, and L. Laurentino, "Optimization of cadmium adsorption using poultry litter biochar through response surface methodology," Chemical Engineering Transactions, Vol. 86, pp. 1507–1512, 2021. https://doi.org/10.3303/CET2186252.

[56]. D. Zhou, S. Ghosh, D. Zhang, N. Liang, X. Dong, M. Wu, and B. Pan, "Role of ash content in biochar for copper immobilization," Environmental Engineering Science, Vol. 33(12), pp. 962–969, 2016. https://doi.org/10.1089/ees.2016.004.

[57]. Turkish Ministry of Agriculture and Forestry, "The parameters required to be examined for 'Poultry Solid Animal Manure' specified in the Regulation on Organic, Mineral and Microbial Source Fertilizers Used in Agriculture Annex-19 Analysis Methods (Official Gazette No. 30341)," 2018. [Online]. Available: https://www.mevzuat.gov.tr/File/GeneratePdf?mevzuatNo=24410&mevzuatTur=KurumVeKurulusYonetmeligi&mevzuatTertip=5. [Accessed: 12 Oct. 2024].

[58]. A. Tomczyk, Z. Sokołowska, and P. Boguta, "Biochar physicochemical properties: pyrolysis temperature and feedstock kind effects," Reviews in Environmental Science and Biotechnology, Vol. 19, pp. 191–215, 2020. https://doi.org/10.1007/s11157-020-09523-3.

[59]. C. Yang, J. Liu, and S. Lu, "Pyrolysis temperature affects pore characteristics of rice straw and canola stalk biochars and biochar-amended soils," Geoderma, Vol. 397, p. 115097, 2021. https://doi.org/10.1016/j.geoderma.2021.115097.

[60]. Y. J. Zhang, Z. J. Xing, Z. K. Duan, M. Li, and Y. Wang, "Effects of steam activation on the pore structure and surface chemistry of activated carbon derived from bamboo waste," Applied Surface Science, Vol. 315, pp. 279–286, 2014. https://doi.org/10.1016/j.apsusc.2014.07.126.

[61]. B. Cagnon, X. Py, A. Guillot, and F. Stoeckli, "The effect of the carbonization/activation procedure on the microporous texture of the subsequent chars and active carbons," Microporous and Mesoporous Materials, Vol. 57(3), pp. 273–282, 2003. https://doi.org/10.1016/S1387-1811(02)00597-8.

[62]. M. S. Shafeeyan, W. M. A. W. Daud, A. Houshmand, and A. Shamiri, "A review on surface modification of activated carbon for carbon dioxide adsorption," Journal of Analytical and Applied Pyrolysis, Vol. 89(2), pp. 143–151, 2010. https://doi.org/10.1016/j.jaap.2010.07.006.

[63]. ICDD, "International Centre for Diffraction Data," 2025. [Online]. Available: https://www.icdd.com/.

[64]. M. C. Morris, H. F. McMurdie, E. H. Evans, B. Paretzkin, H. S. Parker, N. Pyrros, and C. R. Hubbard, Standard X-Ray Diffraction Powder Patterns, U.S. National Bureau of Standards, 1982.

[65]. RRUFF, "Sylvite," 2024. [Online]. Available: https://rruff.info/Sylvite. [Accessed: 13 Oct. 2024].

[66]. S. Yousefi, B. Ghasemi, and M. P. Nikolova, "Opto-structural characterization of Mg(OH)2 and MgO nanostructures synthesized through a template-free sonochemical method," Applied Physics A, Vol. 127(7), p. 549, 2021. https://doi.org/10.1007/s00339-021-04605-7.

[67]. T. B. Tran, S. Hayun, A. Navrotsky, and R. H. R. Castro, "Transparent nanocrystalline pure and Ca-doped MgO by spark plasma sintering of anhydrous nanoparticles," Journal of the American Ceramic Society, Vol. 95(4), pp. 1185–1188, 2012. https://doi.org/10.1111/j.1551-2916.2012.05103.x.

[68]. A. Mbarek, M. Derbel, and G. Chadeyron, "VUV-UV photoluminescence, site occupancy and thermal stability of blue-emitting K2CaP2O7:Eu2+ UV-LED phosphor," Journal of Materials Science: Materials in Electronics, Vol. 32, pp. 21021–21031, 2021. https://doi.org/10.1007/s10854-021-06587-x.

[69]. O. A. Zelekew, S. G. Aragaw, F. K. Sabir, D. M. Andoshe, A. D. Duma, D. H. Kuo, and F. G. Aga, "Green synthesis of Co-doped ZnO via the accumulation of cobalt ion onto Eichhornia crassipes plant tissue and the photocatalytic degradation efficiency under visible light," Materials Research Express, Vol. 8(2), p. 025010, 2021. https://doi.org/10.1088/2053-1591/abe2d6.

[70]. X. Xie, K. Hou, B. Yang, and X. Tong, "Activation of sphalerite by ammoniacal copper solution in froth flotation," Journal of Chemistry, p. 7614890, 2016. http://dx.doi.org/10.1155/2016/7614890.

[71]. H. Barik, M. A. Qaiyum, B. Dey, et al., "Integrated activation strategy of mahua seed cake for efficient wastewater treatment: a sustainable approach for methylene blue removal," Biomass Conversion and Biorefinery, 2024. https://doi.org/10.1007/s13399-024-06040-z.

[72]. F. Wang, W. Yang, P. Cheng, S. Zhang, S. Zhang, W. Jiao, and Y. Sun, "Adsorption characteristics of cadmium onto microplastics from aqueous solutions," Chemosphere, Vol. 235, pp. 1073–1080, 2019. https://doi.org/10.1016/j.chemosphere.2019.06.196.

[73]. M. M. Udawatta, R. C. L. De Silva, and D. S. M. De Silva, "Facile, green approach for aqueous methylene blue dye adsorption: Coconut vinegar treated Trema orientalis

wood biochar," Environmental Engineering Research, Vol. 28(5), pp. 161–173, 2023. https://doi.org/10.4491/eer.2022.617.

[74]. C. Waghmare, S. Ghodmare, K. Ansari, F. M. Alfaisal, S. Alam, M. A. Khan, and Y. Ezaier, "Adsorption of methylene blue dye onto phosphoric acid-treated pomegranate peel adsorbent: Kinetic and thermodynamic studies," Desalination and Water Treatment, p. 100406, 2024. https://doi.org/10.1016/j.dwt.2024.100406.

[75]. A. H. Jawad, N. H. Mamat, M. F. Abdullah, and K. Ismail, "Adsorption of methylene blue onto acid-treated mango peels: kinetic, equilibrium and thermodynamic study," Desalination and Water Treatment, Vol. 59, pp. 210–219, 2017. https://doi.org/10.5004/dwt.2016.0097.

[76]. S. J. Olusegun and N. D. Mohallem, "Comparative adsorption mechanism of doxycycline and Congo red using synthesized kaolinite supported CoFe2O4 nanoparticles," Environmental Pollution, Vol. 260, p. 114019, 2020. https://doi.org/10.1016/j.envpol.2020.114019.

[77]. T. Maneerung, J. Liew, Y. Dai, S. Kawi, C. Chong, and C. H. Wang, "Activated carbon derived from carbon residue from biomass gasification and its application for dye adsorption: kinetics, isotherms and thermodynamic studies," Bioresource Technology, Vol. 200, pp. 350–359, 2016. https://doi.org/10.1016/j.biortech.2015.10.047.

[78]. B. Zhang, Y. Wu, and L. Cha, "Removal of methyl orange dye using activated biochar derived from pomelo peel wastes: performance, isotherm, and kinetic studies," Journal of Dispersion Science and Technology, Vol. 41, pp. 125–136, 2020. https://doi.org/10.1080/01932691.2018.1561298.

[79]. D. T. Hermann, S. Tome, V. O. Shikuku, J. B. Tchuigwa, A. Spieß, C. Janiak, and D. D. Joh Dina, "Enhanced performance of hydrogen peroxide modified pozzolan-based geopolymer for abatement of methylene blue from aqueous medium," Silicon, Vol. 14(10), pp. 5191–5206, 2022. https://doi.org/10.1007/s12633-021-01264-4.

[80]. T. A. Aragaw and A. N. Alene, "A comparative study of acidic, basic, and reactive dyes adsorption from aqueous solution onto kaolin adsorbent: Effect of operating parameters, isotherms, kinetics, and thermodynamics," Emerging Contaminants, Vol. 8, pp. 59–74, 2022. https://doi.org/10.1016/j.emcon.2022.01.002.

[81]. Y. Hu, T. Guo, X. Ye, Q. Li, M. Guo, H. Liu, and Z. Wu, "Dye adsorption by resins: Effect of ionic strength on hydrophobic and electrostatic interactions," Chemical Engineering Journal, Vol. 228, pp. 392–397, 2013. https://doi.org/10.1016/j.cej.2013.04.116.

[82]. L. Mouni, L. Belkhiri, J. C. Bollinger, A. Bouzaza, A. Assadi, A. Tirri, and H. Remini, "Removal of methylene blue from aqueous solutions by adsorption on kaolin: Kinetic and equilibrium studies," Applied Clay Science, Vol. 153, pp. 38–45, 2018. https://doi.org/10.1016/j.clay.2017.11.034.

[83]. S. Debnath, A. Maity, and K. Pillay, "Impact of process parameters on removal of Congo red by graphene oxide from aqueous solution," Journal of Environmental Chemical Engineering, Vol. 2(1), pp. 260–272, 2014. https://doi.org/10.1016/j.jece.2013.12.018.

[84]. S. Basu, G. Ghosh, and S. Saha, "Adsorption characteristics of phosphoric acid induced activation of bio-carbon: Equilibrium, kinetics, thermodynamics and batch adsorber design," Process Safety and Environmental Protection, Vol. 117, pp. 125–142, 2018. https://doi.org/10.1016/j.psep.2018.04.015.

[85]. M. A. Franciski, E. C. Peres, M. Godinho, D. Perondi, E. L. Foletto, G. C. Collazzo, and G. L. Dotto, "Development of CO2 activated biochar from solid wastes of a beer industry and its application for methylene blue adsorption," Waste Management, Vol. 78, pp. 630–638, 2018. https://doi.org/10.1016/j.wasman.2018.06.040.

[86]. M. A. A. Zaini, M. Zakaria, S. H. Setapar, and M. A. Che-Yunus, "Sludge-adsorbents from palm oil mill effluent for methylene blue removal," Journal of Environmental Chemical Engineering, Vol. 1(4), pp. 1091–1098, 2013. https://doi.org/10.1016/j.jece.2013.08.026.

[87]. K. N. Mahmud, T. H. Wen, and Z. A. Zakari, "Activated carbon and biochar from pineapple waste biomass for the removal of methylene blue," Environmental Toxicology and Management, Vol. 1(1), pp. 30–36, 2021. https://doi.org/10.33086/etm.v1i1.2036.

[88]. A. Chaoui, S. Farsad, A. B. Hamou, A. Amjlef, N. Nouj, M. Ezzahery, and N. El Alem, "Reshaping environmental sustainability: Poultry by-products digestate valorization for enhanced biochar performance in methylene blue removal," Journal of Environmental Management, Vol. 351, p. 119870, 2024. https://doi.org/10.1016/j.jenvman.2023.119870.

[89]. M. A. Ahmad, N. A. A. Puad, and O. S. Bello, "Kinetic, equilibrium and thermodynamic studies of synthetic dye removal using pomegranate peel activated carbon prepared by microwave-induced KOH activation," Water Resources and Industry, Vol. 6, pp. 18–35, 2014. https://doi.org/10.1016/j.wri.2014.06.002.

[90]. T. Handayani, P. Ramadhani, and R. Zein, "Modelling studies of methylene blue dye removal using activated corn husk waste: Isotherm, kinetic and thermodynamic evaluation," South African Journal of Chemical Engineering, Vol. 47, pp. 15–27, 2024. https://doi.org/10.1016/j.sajce.2023.10.003.

[91]. J. De Souza Macedo, N. B. da Costa Júnior, L. E. Almeida, E. F. da Silva Vieira, A. R. Cestari, I. de Fátima Gimenez, and L. S. Barreto, "Kinetic and calorimetric study of the adsorption of dyes on mesoporous activated carbon prepared from coconut coir dust," Journal of Colloid and Interface Science, Vol. 298(2), pp. 515–522, 2006. https://doi.org/10.1016/j.jcis.2006.01.021.

[92]. F. Rozada, L. F. Calvo, A. I. García, J. Martín-Villacorta, and M. Otero, "Dye adsorption by sewage sludge-based activated carbons in batch and fixed-bed systems," Bioresource Technology, Vol. 87(3), pp. 221–230, 2003. https://doi.org/10.1016/S0960-8524(02)00243-2.

[93]. Y. C. Sharma, Uma, and S. N. Upadhyay, "An economically viable removal of methylene blue by adsorption on activated carbon prepared from rice husk," Canadian Journal of Chemical Engineering, Vol. 89(2), pp. 377–383, 2011. https://doi.org/10.1002/cjce.20393.

[94]. F. Güleç, O. Williams, E. T. Kostas, A. Samson, L. A. Stevens, and E. Lester, "A comprehensive comparative study on methylene blue removal from aqueous solution using biochars produced from rapeseed, whitewood, and seaweed via different thermal conversion technologies," Fuel, Vol. 330, p. 125428, 2022. https://doi.org/10.1016/j.fuel.2022.125428.

Appendix A. Supplementary Data

Table S1. Energy Dispersive Spectrometry (EDS) results of the AC samples and biochar

051HPLWAC800		PLWCAC800		11ZPLWAC800		Biochar	
Element	**Weight%**	**Element**	**Weight%**	**Element**	**Weight%**	**Element**	**Weight%**
C	45.0	C	54.9	C	75.9	C	34.3
N	3.63	N	3.44	N	5.74	N	5.91
O	17.9	O	19.2	O	6.57	O	22.0
Mg	0.89	Mg	2.17	Al	0.38	P	3.65
Si	0.71	Si	1.09	P	1.85	S	3.33
P	10.2	P	3.92	S	3.26	K	16.9
S	2.12	S	2.05	Cl	1.44	Ca	6.52
K	9.19	K	1.67	Zn	4.83	Mg	1.50
Ca	2.38	Ca	10.23				
Zn	7.95	Fe	0.96				

Table S2. Adsorption isotherms

	Langmiur Isotherm			Freundlich Isotherm		
Samples	**Q_o (mg/g)**	**b (L/mg)**	**R^2**	**k (L/g)**	**n**	**R^2**
051HPLWAC800	48.6	0.025	0.969	7.1	2.97	0.961
11ZPLWAC800	75.5	0.989	0.998	49.5	9.9	0.666
CPLWAC800	119.3	1.1	0.997	78.1	9.8	0.847
Biochar	62.2	2.5	0.97	31.1	5.7	0.473

Table S3. Important parameters of kinetic models

	Pseudo First Order Kinetic Model				Pseudo Second Order Kinetic Model			
Samples	**q_{eth}(mg/g)**	**q_{eex}(mg/g)**	**k_1 (min^{-1})**	**R^2**	**q_{eth}(mg/g)**	**q_{eex}(mg/g)**	**k_2(min^{-1})**	**R^2**
051HPLWAC800 - 25 °C	32.1	39.7	$2.3x10^{-3}$	0.901	26.4	39.7	$6.5x10^{-4}$	0.886
051HPLWAC800 - 35 °C	25.1	34.9	$3.3x10^{-3}$	0.930	28.8	34.9	$7.7x10^{-4}$	0.981
051HPLWAC800 - 45 °C	43.5	50.9	$1.9x10^{-3}$	0.945	30.9	50.9	$4.6x10^{-4}$	0.898
11ZPLWAC800 - 25 °C	45.0	71.4	$4.1x10^{-3}$	0.950	63.3	71.4	$4.9x10^{-4}$	0.995
11ZPLWAC800 - 35 °C	42.8	65.8	$3.6x10^{-3}$	0.934	55.9	65.8	$5.3x10^{-4}$	0.991
11ZPLWAC800 - 45 °C	46.9	74.9	$6.1x10^{-3}$	0.978	73.9	74.9	$3.9x10^{-4}$	0.984
CPLWAC800 - 25 °C	40.9	71.7	$2.2x10^{-2}$	0.969	75.1	71.7	$9.7x10^{-4}$	0.999
CPLWAC800 - 35 °C	21.7	75.0	$2.4x10^{-2}$	0.790	76.6	75.0	$2.2x10^{-3}$	0.999
CPLWAC800 - 45 °C	14.3	74.8	$2.2x10^{-2}$	0.817	76.1	74.8	$3.1x10^{-3}$	0.999
Biochar - 25 °C	23.8	41.0	$5.9x10^{-3}$	0.862	39.3	41.0	$1.0x10^{-3}$	0.992
Biochar - 35 °C	22.5	51.3	$6.2x10^{-3}$	0.966	49.9	51.3	$1.2x10^{-3}$	0.997
Biochar - 45 °C	26.1	56.1	$3.2x10^{-3}$	0.651	47.7	56.1	$1.2x10^{-3}$	0.989